RSC Advances

PAPER

View Article Online
View Journal | View Issue

Cite this: *RSC Adv.*, 2016, **6**, 104529

Study on the structural and electrocatalytic properties of Ba^{2+}- and Eu^{3+}-doped silica xerogels as sensory platforms†

Paulo A. Raymundo-Pereira,[abc] Diego A. Ceccato,[ab] Airton G. B. Junior,[ab] Marcos F. S. Teixeira,[ab] Sergio A. M. Lima[ab] and Ana. M. Pires*[ab]

Received 8th September 2016
Accepted 17th October 2016

DOI: 10.1039/c6ra22508j

www.rsc.org/advances

This work reports on the sol–gel synthesis of barium- and europium-doped silica xerogel and its use as an electrocatalytic sensor. Barium was chosen to assist the network framing and europium to provide electronic properties, including the Eu^{2+}/Eu^{3+} redox process. The results from different molecular and structural techniques indicated that this xerogel is a composite material that combines a non-crystalline polymeric silica network with a high level of agglomeration and a low degree of reticulation formed by the hydrolysis and condensation of TEOS and M–O bonds (M = Ba^{2+} and/or Eu^{3+}), whereas the oxygen atoms belong to the xerogel phase. The electrochemical behavior of the silica xerogel:Ba^{2+},Eu^{3+} with different amounts of Eu^{3+} under several different conditions was investigated. The electrochemical sensing platform showed a well-defined redox coupling with a formal potential of 0.06 V, assigned to europium redox sites in silicate. Electrocatalytic activity was observed with an increasing anodic peak current to the isoniazid oxidation, indicating that the electrochemical sensing platform designed here was successfully achieved.

1. Introduction

The development of electrocatalytic devices has been an area that has seen great advancement in recent years[1–10] due to their low cost of instrumentation and the possibility of being assembled by different materials,[1–12] with several reviews found in the literature.[11,13–15] Furthermore, by adding different chemical species to the electrode surface, electron transfer in slow electrochemical reactions is facilitated[9] as the physicochemical nature of the electrode/solution interface is changed. The operation mechanism of these devices depends on the properties of the material immobilized at the electrode surface to promote electron transfer toward the target species.[16] Carbon paste electrodes (CPEs) have been extensively applied for this purpose since their surfaces are easily modified.[9] Electrocatalytic devices based on CPE have been widely applied toward the determination of trace amounts of elements, the evaluation of electrochemical processes, the preparation of biosensors, and the investigation of electrocatalytic mechanisms and organic species.[1–10]

Lanthanides are very versatile and can be used in the production of glasses, ceramics,[17] alloys, and electronics, and they also find application in agriculture and natural sciences.[18] Lanthanide luminescent-based chemical and biological sensors have been highlighted due to their photophysical properties and their selective emission response to specific analytes.[19–23] Despite the huge and increasing number of applications using rare earth ions, proportionally there are few studies related to the development and use of rare earth-based electrocatalysts for sensors;[3,11,24–34] nonetheless, this application should be explored due to the excellent catalytic behavior that lanthanides exhibit.

Silica xerogels obtained from the sol–gel method have been the focus of attention for electrochemists because of their advantageous features, such as mechanical stability, durability, and the possibility of doping them with metal cations.[35] In this context, our strategy was to develop a carbon paste electrode modified with a composite material that would combine a high surface area and high porosity allied with the peculiar electronic properties of europium ions. Despite the fact that 3+ is the most stable oxidation state for europium, depending on the chemical environment, europium can be stabilized in its reduced atypical 2+ state. Therefore, due to having a similar ionic radius and the same charge, Ba^{2+} was chosen as the network polymeric frame in order to provide suitable sites to stabilize Eu^{2+} ions, thus favoring the electrochemical Eu^{3+}/Eu^{2+} redox process.[36] To fulfill the physical characteristics of the material, the chosen

[a]*Faculdade de Ciências e Tecnologia, UNESP – Univ Estadual Paulista, Rua Roberto Simonsen, 305, 19060-900, Presidente Prudente, SP, Brazil. E-mail: anapires@fct.unesp.br; Tel: +55 1832295748*

[b]*Instituto de Biociências, Letras e Ciências Exatas, UNESP – Univ Estadual Paulista, Rua Cristóvão Colombo, 2265, 15054-000 São José do Rio Preto, SP, Brazil*

[c]*Instituto de Química de São Carlos, Universidade de São Paulo-USP, São Carlos, SP, 13566-590, Brazil*

† Electronic supplementary information (ESI) available. See DOI: 10.1039/c6ra22508j

synthesis method was the sol–gel method.[37–39] Finally, in order to evaluate the potential of this system for use in sensing devices, the electrocatalytic activity of the silica xerogel:Ba,Eu was explored to identify isoniazid molecules in physiological media.

2. Experimental section

2.1 Synthesis of silica xerogel:Ba^{2+},Eu^{3+} *via* the sol–gel route

Silica xerogels containing Ba^{2+} and Eu^{3+} (xerogel:Ba^{2+},Eu^{3+}) were synthesized *via* the sol–gel route by using $Ba(CH_3COO)_2$ (VETEC, 99.9%), Eu_2O_3 (Aldrich, 99.99%), $C_8H_{20}O_4Si$, (TEOS, Fluka, 99.9%), and CH_3COOH (VETEC, 97%) as the starting reagents. A sample containing only barium, *i.e.*, silica xerogel:Ba^{2+}, was prepared as a control sample. The amount of Ba^{2+} ions was kept constant by using 2eq$Ba(CH_3COO)_2$:1eqTEOS, while the amount of Eu^{3+} ions was varied relative to the Ba^{2+} ions as 0.5, 1.0, 5.0, and 10 ch% (charge percentage). Here, we considered an isoelectronic doping process or charge compensation mechanism (CCM), since Ba^{2+} and Eu^{3+} have different charges, whereby for each three Ba^{2+} ions taken, we introduced two Eu^{3+} ions, so the total positive charge remained unchanged.

For the gel synthesis, stoichiometric amounts of barium and europium acetates dissolved in 10 mL of acetic acid and TEOS in an isopropyl alcohol solution (5.55×10^{-1} mol L^{-1}) were used as the starting reagents ($2Ba^{2+}$:1 TEOS). The doping percentage was calculated in relation to Ba^{2+} ions. Then, 0.4 mL of deionized water was added to the mixture to initiate the hydrolysis reactions. Acetic acid was also added and acted as a solvent and catalyst. The mixture was kept under stirring for 6 h at room temperature until gel formation. The gel was thermally treated at 100 °C in a static air atmosphere for 2 h to allow solvent evaporation, resulting in the xerogel phase. Then, the silica xerogel:Ba^{2+},Eu^{3+} (1.0 ch%) sample was calcinated at 100, 200, 300 or 400 °C in an O_2 atmosphere with a heating ramp of 5 °C min^{-1} for 2 h in an EDG muffle furnace type.

2.2 Structural and molecular characterization

The produced xerogel samples were used to develop a sensory platform, and their electrochemical performance were investigated by using cyclic voltammetry. The influence of several parameters, such as pH, oxidizing atmosphere, supporting electrolyte, europium amount (%), and potential scan rate, on the electrochemical behavior of the silica xerogel:Ba^{2+},Eu^{3+} were analyzed by the cyclic voltammetry. The sample xerogel:Ba^{2+},Eu^{3+} (1.0%) calcinated at 100 °C was also characterized by Fourier Transform Infrared Spectroscopy (FTIR) using a Shimadzu Spectrometer IR Affinity-1 model; by scanning electron microscopy (SEM) using a Carls Zeiss model EVO LS15 scanning electron microscope with a detector of secondary electron (SE) in a high vacuum and at constant temperature; and by thermal analysis using a Universal V45A TA Instruments, no flow of air, and a heating ramp of 10 °C min^{-1} up to 1200 °C. Solid-state NMR of $^{29}Si\{^1H\}$ cross-polarization experiments were conducted using a Bruker Avance spectrometer at a magnetic field of 9.4. The $^{29}Si\{^1H\}$ CP-MAS spectra were measured under a spinning speed of 10 kHz and using a CP contact time of 2.5 ms and relaxation delay of 5 s. All the spectra were acquired with TPPM proton decoupling during the data acquisition applying decoupling pulses. Chemical shifts are reported herein relative to the TMS referencing standard.

2.3 Preparation of electrocatalytic devices with silica xerogel:Ba^{2+},Eu^{3+}

As described elsewhere,[24,40] the modified carbon paste electrode (MCPE) used to set up the sensory platform was prepared by carefully mixing 55 wt% of graphite powder (1–2 μm particle size, Aldrich), 25 wt% silica xerogel:Ba^{2+},Eu^{3+} with different percentages of Eu^{3+} (0, 0.5, 1.0, 5.0, or 10 ch%), and 20 wt% of mineral oil (Aldrich), for a total mass of 0.5 g. This mixture was prepared under magnetic stirring in a Becker (50 mL) containing 20 mL of hexane. The final paste was obtained by evaporation of the solvent. The modified carbon paste was packed into an electrode body, consisting of a plastic cylindrical tube (o.d. 7 mm, i.d. 4 mm) equipped with a stainless steel staff serving as an external electric contact. Appropriate packing was achieved by pressing the electrode surface (surface area of 12.6 mm^2) against a filter paper.

2.4 Reagents and solutions for electrochemical assays

All the solutions were prepared using water purified with a Millipore Milli-Q system. All the chemicals were of analytical grade and used without further purification. The supporting electrolyte used for the initial experiments was a 0.1 mol L^{-1} KCl solution. The isoniazid (1.0×10^{-3} mol L^{-1}) was prepared in solutions of NaCl 0.1 mol L^{-1}, and then used as the storage solution. The solutions were purged with nitrogen to remove dissolved oxygen before the measurements.

2.5 Voltammetric apparatus

All the voltammetric measurements were carried out in a 50 mL thermostatted glass cell at 25 °C with a three-electrode configuration: a sensory platform as the working electrode, a saturated calomel electrode (SCE) as the reference electrode, and platinum wire as the auxiliary electrode. During the measurements, the solution in the cell was neither stirred nor aerated. The measurements were conducted with a μAutolab type III (Eco Chimie) connected to a microcomputer and controlled by GPES software.

3. Results and discussion

3.1 Silica xerogel doped samples characterization

Thermogravimetric (TG) and differential scanning calorimetry (DSC) analyses for the silica xerogel:Ba^{2+},Eu^{3+} (1.0 ch%) and xerogel:Ba^{2+} samples showed a mass loss of approximately 5%, with exothermic peaks around 450 °C related to the formation of barium carbonate, and an endothermic peak at 1100 °C with no mass loss related to the formation of barium silicate (Fig. 1). X-ray diffraction patterns recorded for the xerogel:Ba^{2+} sample heated under 450 °C and another one heated under 1100 °C

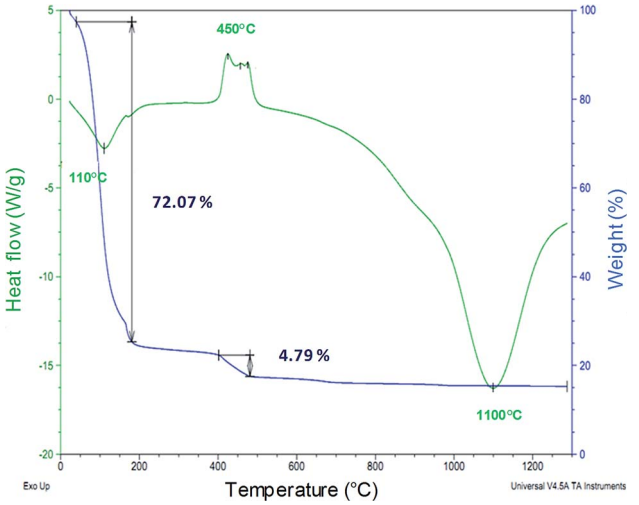

Fig. 1 Thermogravimetric (TG) and differential scanning calorimetry (DSC) analyses for the silica xerogel:Ba^{2+},Eu^{3+} (1 ch%) sample.

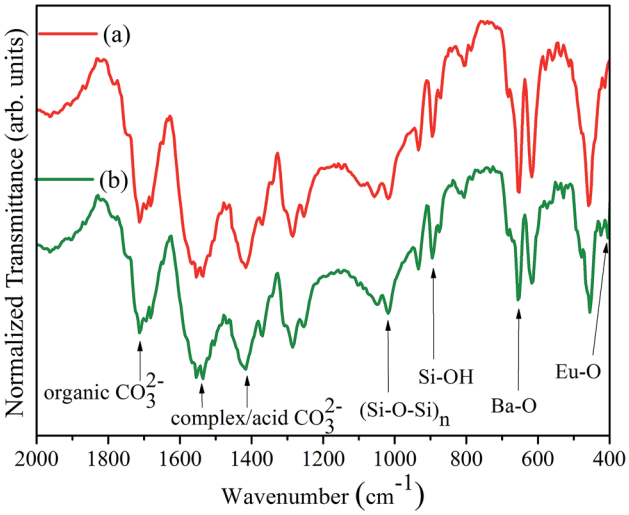

Fig. 2 FTIR spectra of (a) silica xerogel:Ba^{2+} and (b) silica xerogel:Ba^{2+},Eu^{3+} (1 ch%), both in KBr pellets.

supports this phase assignment, and can be found in the ESI, S1.†

The solid-state ^{29}Si NMR spectra for the silica xerogel:Ba^{2+} and silica xerogel:Ba^{2+},Eu^{3+} (1.0 ch%) samples treated at 100 °C, as seen in Fig. S2(a) and (b),† exhibit three peaks, each at −90.70 (−92.98) ppm, −104.38 (−103.60) ppm, and −112.35 (−111.96) ppm, assigned to the $Si(OSi)_2(OH)_2$ group (Q^2), $Si(OSi)_3(OH)$ group (Q^3), and $Si(OSi)_4$ group (Q^4), respectively, all corresponding to the inorganic polymeric structure of silica.[41] Since the CP-MAS ($^{29}Si\{^1H\}$) cross-polarization acquisition mode was used, those groups that have hydrogen atoms near by the silicon nucleus are intensified; therefore, in both samples, the most intense signal corresponds to the Q^3 site. Probably, the $Si(OSi)_3(OH)$ groups are on the xerogels surface. The intensity of the signal assigned to the Q^2 groups apparently increases for the sample containing europium, but this could be associated with the europium paramagnetic effect on the silica surface causing a signal loss.

In the FTIR spectra of the silica xerogel:Ba^{2+} and silica xerogel:Ba^{2+},Eu^{3+} (1 ch%) samples, as seen in Fig. 2, bands centered near 1014 cm^{-1} and 892 cm^{-1} assigned to the $(Si\text{–}O\text{–}Si)_n$ and Si–OH vibration modes, respectively, can be observed, which confirms the formation of polymeric silica as a result of TEOS hydrolysis and condensation. Also, the presence of vibration modes with an energy lower than 700 cm^{-1} related to M–O bonds (M = Eu^{3+} and/or Ba^{2+}) ensure that metallic ions are combined to oxygen atoms in the xerogel network. Bands centered near 1550, 1420, and 1280 cm^{-1} indicate the presence of carbonates in the xerogel structure namely originating from the thermal decomposition of acetic acid.

SEM images of the silica xerogel:Ba^{2+} and silica xerogel:Ba^{2+},Eu^{3+} (1 ch%) samples treated at 100 °C, as seen in Fig. 3, show that both samples exhibit a high level of agglomeration. According to Rios *et al.*,[42] the presence of non-hydrolyzable groups from TEOS leads to a xerogel with a lower degree of reticulation.[42]

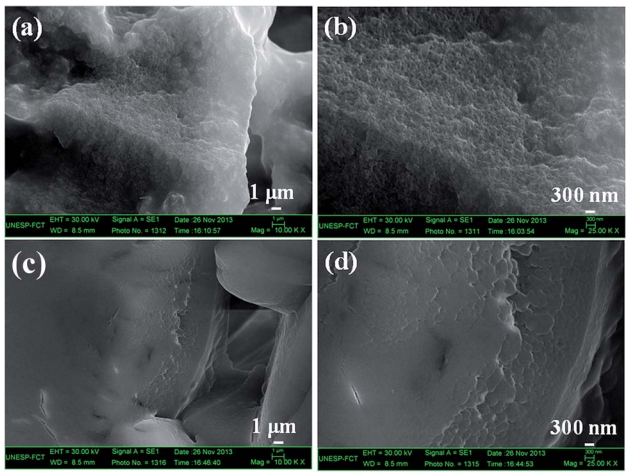

Fig. 3 SEM images of silica xerogel:Ba^{2+} (a) and (b); and silica xerogel:Ba^{2+},Eu^{3+} (1 ch%) (c) and (d).

3.2 Influence of the silica xerogel:Ba^{2+},Eu^{3+} synthesis conditions on the sensory platform electrochemical performance

To assess the effect of the europium doping concentration in the silica xerogel:Ba^{2+},Eu^{3+} on the sensory platform, all the samples were prepared by heating the gel at 100 °C for 2 h. Voltammetric profiles were evaluated in 0.1 mol L^{-1} KCl solution at pH 5.8, while the cyclic scans were conducted in the unstirred solution at a potential scan rate of 50 mV s^{-1} from −0.50 to +0.50 V *vs.* SCE, recording first the oxidation step and then the reduction step in the presence of oxygen. All the voltammograms shown in Fig. 4 were recorded in similar conditions. Fig. 4(a) shows the influence of the amount of Eu^{3+} ions varying from 0.5 ch% up to 10 ch% in the silica xerogel:Ba^{2+},Eu^{3+} phase on the anodic and cathodic peak current signal of the sensory platform. A defined current peak can only

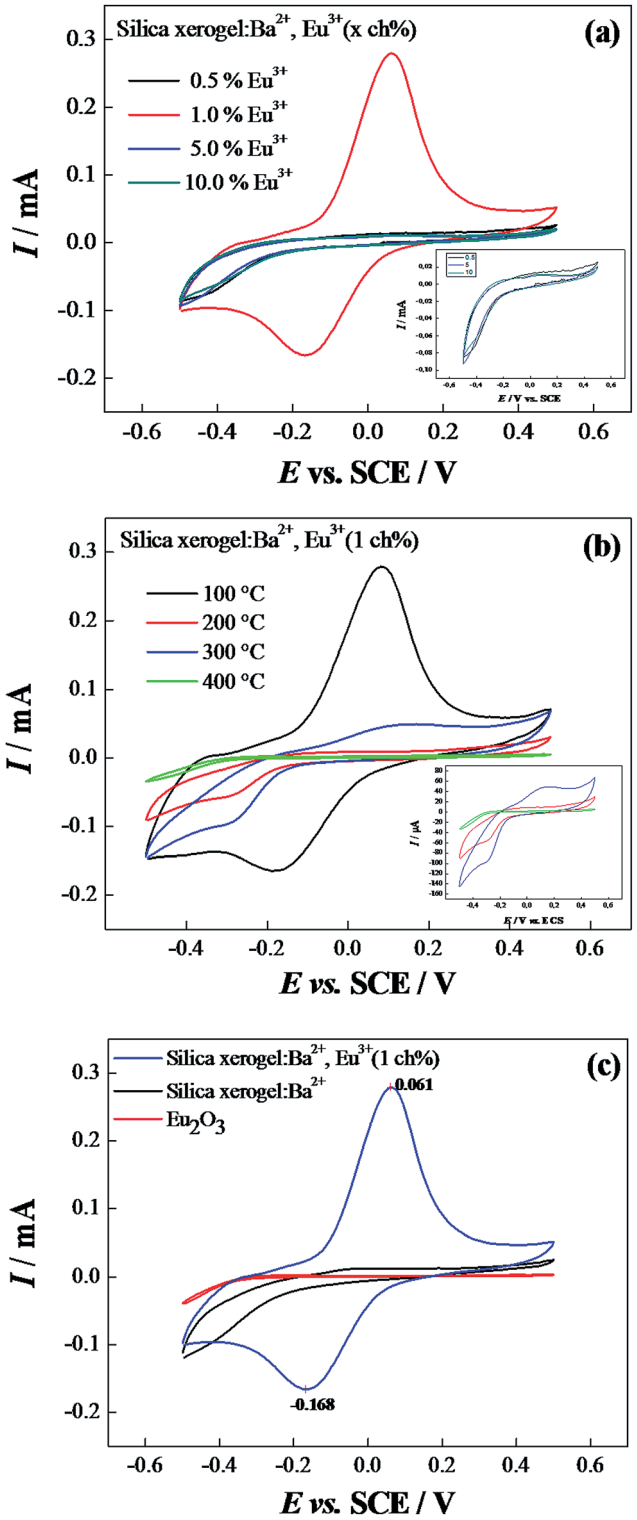

Fig. 4 Cyclic voltammograms obtained at a potential scan rate of 50 mV s^{-1} between +0.5 and −0.5 V *vs.* SCE in the presence of oxygen for the sensory platform with: (a) silica xerogel:Ba^{2+},Eu^{3+} containing 0.5, 1.0 5.0, or 10 ch% of Eu^{3+} ions; (b) xerogel:Ba^{2+},Eu^{3+} (1 ch%) pretreated thermally at 100–400 °C; and (c) silica xerogel:Ba^{2+}, xerogel:Ba^{2+},Eu^{3+} (1 ch%), and Eu_2O_3.

be observed for the sample containing 1.0 ch% of Eu^{3+} ions in the xerogel. When the concentration is higher than 1.0 ch%, the ionic mobility in the electrode surface is blocked, making the electron transfer process difficult in the xerogel, consequently suppressing the electrochemical process in the electrode surface. For lower concentrations, *e.g.*, the 0.5 ch% sample, we observe that the electrochemical process does not take place; probably the amount of active species is not enough to promote the oxidation/reduction processes at the surface when the potential scan is applied onto the sensory platform. Thus, the silica xerogel:Ba^{2+},Eu^{3+} containing 1.0 ch% of Eu^{3+} ions was selected for the further studies because it exhibited the best voltammetric profile with a well-defined peak potential. The silica xerogel:Ba^{2+},Eu^{3+} (1 ch%) sample was thermally treated at different temperatures prior to the preparation of the sensory platform, and the results are shown in Fig. 4(b). It is possible to observe that the anodic and cathodic peak currents dramatically decrease for the sensory platform prepared with the silica xerogel samples that were heat-treated under higher temperatures, even disappearing completely for the sensory platform with the xerogel treated at 400 °C. By increasing the treatment temperature, the xerogel gradually acquires a long distance organization, creating a crystalline structure, whereas europium ions can move to the interstices, thus decreasing its efficiency in terms of the electron transfer process and ion mobility. Thus, Eu^{3+} ions within a crystalline network have difficulty in changing their oxidation state. Consequently, the sensory platform prepared with silica xerogel:Ba^{2+},Eu^{3+} (1 ch%) treated at 100 °C was selected for further investigation. In order to verify if the electrochemical response was due to the composite combined properties or the individual components, in Fig. 4(c) we compare the voltammetric profiles of the sensory platform prepared with silica xerogel:Ba^{2+}, silica xerogel:Ba^{2+},Eu^{3+} (1 ch%), and pure europium(III) oxide (Eu_2O_3). Only the sample containing silica xerogel:Ba^{2+},Eu^{3+} (1 ch%) exhibits a typical cyclic voltammogram, with two peaks at +0.061 V (E_{PA}) and −0.168 V (E_{PC}), both remaining stable after the second cycle, with a quasi-reversible wave with a $\Delta E_P = 229$ mV. The peaks can be attributed to the reversible single-electron-reduction/oxidation process of the Eu^{II}/Eu^{III} pair. This is evidence of Eu redox activity for the electrode, although in general the redox peaks are somewhat ill defined.[43,44]

3.3 General electrochemical properties of the silica xerogel:Ba^{2+},Eu^{3+} sensory platform

The surface concentration of electroactive species (Γ/mol cm^{-2}) was estimated from the background-corrected electric charge (Q), under the anodic peaks in accordance with the theoretical relationship[31] as follows $\Gamma = Q/nFA$, where Q (C) is the background-corrected electric charge, calculated by integrating the anodic peak of the cyclic voltammogram ($v = 5$ mV s^{-1}) in KCl aqueous solution; n is the number of electrons transferred; F is the Faraday constant; and A is the electrode geometric area. The calculated Q value was 1.9×10^{-3} C, and the estimated surface concentration was 1.6×10^{-7} mol cm^{-2}. To determine the influence of the oxygen on the electrochemical behavior of

the sensory platform, some experiments were carried out in degassed solution, and the profile, which is included in the ESI in Fig. S3,† exhibited a marked small alteration in the redox potential in the absence of dissolved O_2 ($\Delta E_{P(presence)-(absence)} =$ 40 mV), while the current values were not altered. Therefore all the analyses were performed in the absence of oxygen. Furthermore, this significant difference in the current magnitude at −0.40 V *vs.* SCE could be assigned to the reduction of dissolved oxygen in solution.[45] Thus, these results indicate that the silica xerogel:Ba^{2+},Eu^{3+} sensory platform has promise as a sensor for dissolved oxygen.

The effect of the potential scan rates (5–300 mV s^{-1}) on the voltammetric response of the silica xerogel:Ba^{2+},Eu^{3+} sensory platform in 0.1 mol L^{-1} KCl solution was also investigated. The recorded cyclic voltammograms revealed that the anodic peak current increases and that the peak potential shifts as the scan rate increases, as shown in Fig. S4.† The anodic and cathodic peak currents varied linearly with the square root of the scan rates (inset Fig. S4†). This linearity indicates that the redox process follows a diffusion-controlled mechanism. This behavior suggests a mobility of the counter-ions of the supporting electrolyte, which is necessary for charge transport or to keep the electroneutrality at the electrode surface during the redox process.[46] Moreover, in Fig. S4 (ESI†), it can be seen well-defined peaks after 300 CV, indicating that the leaching of ions is not observed. In addition, the voltammetric performance of the sensory platform was investigated in different supporting electrolytes: alkaline chlorides (CsCl, RbCl, KCl, NaCl, and LiCl), earth-alkaline chlorides ($BaCl_2$, $SrCl_2$, $CaCl_2$, and $MgCl_2$), and different sodium counter-ions ($NaClO_4$, NaCl, $NaNO_3$, Na_2SO_4, Na_2CO_3, and Na_3PO_4), all at a concentration of 0.1 mol L^{-1}. The potential peaks ($Eu^{(II)}/Eu^{(III)}$) in different alkaline ions decrease with the decrease in the ionic radius (from Cs^+ to Na^+), as indicated in Fig. 5(a). The lithium ions, however, show an anomalous behavior, which can be easily explained by the high degree of hydration hindering the mobility of lithium ions. For the earth-alkaline ions, as seen in Fig. 5(b), the peak potential ($Eu^{(II)}/Eu^{(III)}$) increases in line with the decreasing ionic radius (from Ba^{2+} to Mg^{2+}), demonstrating the counter-ions influence on the voltammetric behavior of the silica xerogel:Ba^{2+},Eu^{3+} for both the alkaline and earth-alkaline ions. The peak potential was found to be linearly dependent upon the ratio [charge]/[radius], indicating the migration of such ions into the silica xerogel:Ba^{2+},Eu^{3+} network. From these results, we assume that a mobility of the supporting electrolyte is necessary for the charge transport and electroneutrality on the electrode surface during the redox process.

The influence of the anions: chloride, acetate, nitrate, perchlorate, sulfate, phosphate, and carbonate in the supporting electrolyte on the voltammetric behavior of the silica xerogel:Ba^{2+},Eu^{3+} sensory platform was also investigated, and the results can be seen in Fig. S5.† When carbonate and phosphate ions were used, the redox process of $Eu^{(II)}/Eu^{(III)}$ disappears because the ions are in their hydrolyzed form, and consequently they are in a lower concentration. We did not find in this study a clear dependence of the [ionic charge]/[ionic radius] ratio with the peak potentials; however, chloride ion had the lowest peak potentials. Therefore, the NaCl 0.1 mol L^{-1} solution was chosen as the best pattern due to its better voltammetric profile, and also because it had the most negative potential observed among the electrolyte solutions.

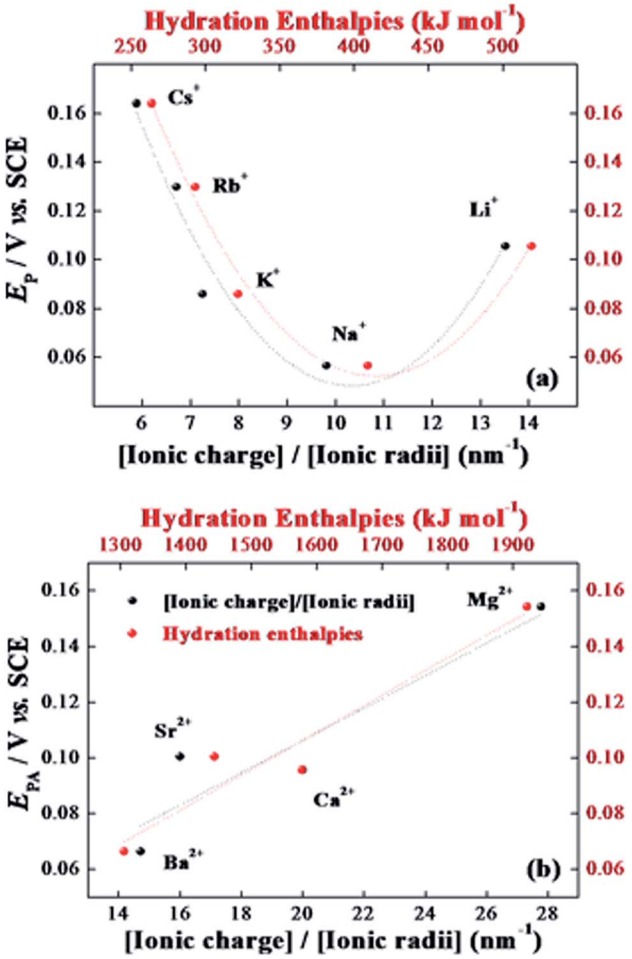

Fig. 5 Evolution of the anodic peak potential of the silica xerogel:Ba^{2+},Eu^{3+} (1 ch%) sensory platform as a function of the [ionic charge]/[ionic radii] and hydration enthalpies for alkaline ions (a) and for earth-alkaline ions (b).

The electrochemical behavior of the silica xerogel:Ba^{2+},Eu^{3+} sensory platform in a 0.10 mol L^{-1} NaCl solution was studied over a pH range of 2.0–12.0 using cyclic voltammetry and a potential scanning from −0.5 to +0.5 V (*vs.* SCE) at a 50 mV s^{-1} scan rate. The electrolytic solutions were adjusted with hydrochloric acid and sodium hydroxide. The experimental results showed that the silica xerogel:Ba^{2+},Eu^{3+} sensory platform is more stable in neutral aqueous solutions than in basic solutions. The voltammetric profile of the silica xerogel:Ba^{2+},Eu^{3+} sensory platform was slightly changed at pH 2–10, which is indicative that the mechanism did not involve a proton transfer process but rather a single electron transfer process under the experimental conditions. For pH levels higher than 10, a single anodic peak of irreversible character was observed for a more positive potential. This behavior is probably more related to the europium hydroxide formation being in equilibrium with the silica xerogel:Ba^{2+},Eu^{3+} on the electrode surface

than to counter-ion influences on the voltammetric performance of the silica xerogel:Ba^{2+},Eu^{3+}. The peak potential and peak current values were related to the pH values but no linear relationship was obtained (Fig. S6†); thus, the pH of the electrolyte solution (*i.e.*, pH 6.0) was selected for the sequencing studies.

3.4 Application of the silica xerogel:Ba^{2+},Eu^{3+} sensory platform for the electrocatalytic oxidation of isoniazid

Voltammetric measurements were carried out in 0.1 mol L^{-1} NaCl solution (pH 6.0) containing different isoniazid concentrations in order to obtain the analytical curve. Fig. 6 illustrates the anodic peak current for different isoniazid concentrations, suggesting an interaction between the silica xerogel: Ba^{2+},Eu^{3+} and isoniazid. The current values (at +0.06 V) obtained provided a linear relationship with the isoniazid concentration ranging from 2.5×10^{-6} to 2.4×10^{-5} mol L^{-1}. From 2.4×10^{-5} mol L^{-1} onwards, a deviation from linearity occurred owing to saturation of the electrode surface.[47]

The increase in the anodic peak current clearly shows the catalytic process of isoniazid oxidation by the central metallic cation in the silica xerogel:Ba^{2+},Eu^{3+}. The suggested interaction is similar to an electrochemical–chemical (EC′) mechanism.[48] Two redox steps can describe the electrocatalytic mechanism of the sensory platform. In the first: when a positive potential higher than 0.061 V *vs.* SCE is applied to the working electrode, an electrochemical oxidation of silica xerogel:Ba^{2+},Eu^{2+} occurs, producing silica xerogel:Ba^{2+},Eu^{3+} on the electrode surface. When the cathodic potential is swept, the silica xerogel:Ba^{2+},Eu^{2+} is electrochemically regenerated. In the second step, the xerogel in the oxidized form reacts with $isoniazid_{red}$ generating $isoniazid_{oxi}$ (see Fig. 6), consequently reducing the silica xerogel:Ba^{2+},Eu^{3+} to silica xerogel:Ba^{2+},Eu^{2+}, which is electrochemically reduced. The increase in the magnitude of the anodic peak current obtained at 0.061 V (*versus* SCE) is proportional to the analyte concentration in solution.

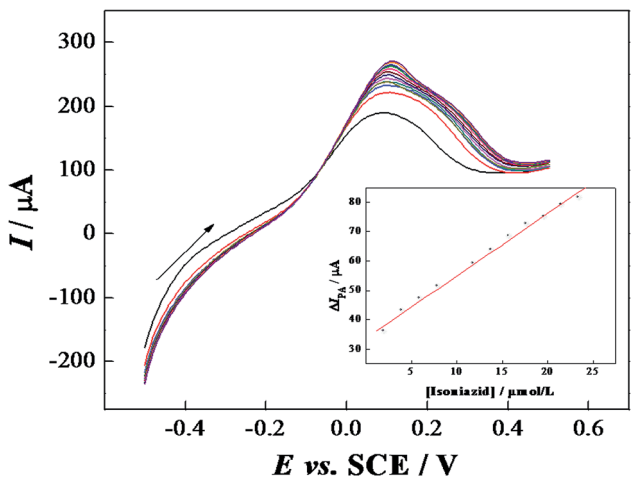

Fig. 6 Linear scan voltammograms obtained at 50 mV s^{-1} for the silica xerogel:Ba^{2+},Eu^{3+} (1 ch%) sensory platform containing different concentrations of isoniazid. In the inset, analytical curves for isoniazid obtained from the voltammograms.

The detection limit was calculated following the method described in the experimental section and the value obtained was 2.91×10^{-7} mol L^{-1}. This low detection limit can be explained by the synergetic effect between the silica xerogel:Ba^{2+},Eu^{3+} and isoniazid, which facilitates the electron transfer. The silica xerogel:Ba^{2+},Eu^{3+} sensory platform exhibited convincing repeatability without a significant loss of electrocatalytic activity, with a relative standard deviation (RSD) lower than 5%. The results showed that the relative standard deviation (RSD) of the peak current of Eu^{2+}/Eu^{3+} varies, where the intra-day repeatability was 3.3% (with $n = 10$), suggesting that the prepared silica xerogel:Ba^{2+},Eu^{3+} sensory platform has good stability. This could be ascribed to the excellent stability and renewability of the surface. When five parallel-fabricated sensors were compared for inter-day repeatability, a relative standard deviation (RSD) of 2.9% was observed, indicating a good reproducibility of the sensor assembling. Moreover, the stability of the sensor was also evaluated. Fifty measurements were recorded and the initial electrochemical response decreased by only 4.9%; these experimental results indicate that the current response is reproducible and that the silica xerogel:Ba^{2+},Eu^{3+} sensory platform possesses long-term stability.

4. Conclusions

A Ba^{2+},Eu^{3+}-doped silica xerogel was fully characterized by TG, DSC, FTIR, SEM, and solid-state ^{29}Si NMR, which showed that it is a composite material that combines a non-crystalline polymeric silica network with a high level of agglomeration and a low degree of reticulation formed by the hydrolysis and condensation of TEOS and M–O bonds (M = Ba^{2+} and/or Eu^{3+}), whereas the oxygen atoms belong to the xerogel phase. Furthermore, cyclic voltammetry data indicated that Eu^{3+} ions present in the xerogel network facilitate the oxidation of isoniazid at lower potentials (0.061 V *vs.* SCE). Therefore, the electrochemical properties of the Ba^{2+},Eu^{3+}-doped silica xerogel in addition to its catalytic ability showed greater efficiency in the isoniazid detection, with the added advantage that the device preparation was not time consuming. Finally, the electrochemical properties of the silica xerogel:Ba^{2+},Eu^{3+} electrochemical sensing platform combined with its high catalytic activity yielded values for the detection limit in the micromolar range, exhibited high reproducibility and repeatability, and excellent sensitivity. In essence, this study highlights the potential improvement involved in the unexploited direct application of an inorganic composite in electrode surface modification. The low cost of the Ba^{2+},Eu^{3+}-doped silica xerogel sensory platform applied to isoniazid electrocatalytic oxidation compared to graphene, carbon nanotubes, or metallic nanoparticles devices, represents a competitive advantage for this device as a suitable tool for electrochemical applications.

Acknowledgements

The authors are thankful to the Brazilian agencies FAPESP, CNPq (302728/2012-0) and CAPES for the financial research support. Paulo A. Raymundo-Pereira is particularly grateful to

the São Paulo research Foundation (FAPESP) for the award of a scholarship (Grant No. 2008/07298-7, 2012/17689-9, 2016/01919-6 and 2015/10394-1). Laboratório de Microscopia Eletrônica de Varredura (FCT-UNESP) and RMN Si (IQ-UNESP, Araraquara).

References

1 L. B. Qu, S. L. Yang, G. Li, R. Yang, J. J. Li and L. L. Yu, Preparation of yttrium hexacyanoferrate/carbon nanotube/Nafion nanocomposite film-modified electrode: Application to the electrocatalytic oxidation of L-cysteine, *Electrochim. Acta*, 2011, **56**, 2934–2940.

2 Q. L. Sheng, H. Yu and J. B. Zheng, Solid state electrochemical of the erbium hexacyanoferrate-modified carbon ceramic electrode and its electrocatalytic oxidation of L-cysteine, *J. Solid State Electrochem.*, 2008, **12**, 1077–1084.

3 K. Farhadi, F. Kheiri and M. Golzan, Th(IV)-hexacyanoferrate modified carbon paste electrode as a new electrocatalytic probe for simultaneous determination of ascorbic acid and dopamine from acidic media, *J. Braz. Chem. Soc.*, 2008, **19**, 1405–1412.

4 T. C. Canevari, J. Arguello, M. S. P. Francisco and Y. Gushikem, Cobalt phthalocyanine prepared in situ on a sol-gel derived SiO_2/SnO_2 mixed oxide: application in electrocatalytic oxidation of oxalic acid, *J. Electroanal. Chem.*, 2007, **609**, 61–67.

5 M. E. Tess and J. A. Cox, Electrocatalysis with a dirhodium-substituted polyoxometalate anchored in a xerogel-based composite: application to the oxidation of methionine and cystine at physiological pH, *Electroanalysis*, 1998, **10**, 1237–1240.

6 M. E. Tess and J. A. Cox, Matrix effects on coupled chemical reactions in solid-state voltammetry: disproportionation of uranium(V) in a silica xerogel, *J. Electroanal. Chem.*, 1998, **457**, 163–169.

7 B. R. Kozub and R. G. Compton, Voltammetric studies of the redox mediator, cobalt phthalocyanine, with regard to its claimed electrocatalytic properties, *Sens. Actuators, B*, 2010, **147**, 350–358.

8 L. S. S. Santos, R. Landers and Y. Gushikem, Application of manganese(II) phthalocyanine synthesized in situ in the SiO_2/SnO_2 mixed oxide matrix for determination of dissolved oxygen by electrochemical techniques, *Talanta*, 2011, **85**, 1213–1216.

9 C. S. Martin and M. F. S. Teixeira, Electrocatalytic study of an electrode modified with Reactive Blue 4 dye covalently immobilized on amine-functionalized silica, *J. Solid State Electrochem.*, 2012, **16**, 3877–3886.

10 M. F. S. Teixeira, F. H. Cincotto and P. A. Raymundo-Pereira, Electrochemical investigation of the dimeric oxo-bridged ruthenium complex in aqueous solution and its incorporation within a cation-exchange polymeric film on the electrode surface for electrocatalytic activity of hydrogen peroxide oxidation, *Electrochim. Acta*, 2011, **56**, 6804–6811.

11 N. R. de Tacconi, K. Rajeshwar and R. O. Lezna, Metal hexacyanoferrates: electrosynthesis, in situ characterization, and applications, *Chem. Mater.*, 2003, **15**, 3046–3062.

12 J. Zima, I. Svancara, J. Barek and K. Vytras, Recent Advances in Electroanalysis of Organic Compounds at Carbon Paste Electrodes, *Crit. Rev. Anal. Chem.*, 2009, **39**, 204–227.

13 B. Uslu and S. A. Ozkan, Electroanalytical Methods for the Determination of Pharmaceuticals: A Review of Recent Trends and Developments, *Anal. Lett.*, 2011, **44**, 2644–2702.

14 B. C. Janegitz, M. Baccarin, P. A. Raymundo-Pereira, F. A. dos Santos, G. G. Oliveira, S. A. S. Machado, M. R. V. Lanza, O. Fatibello and V. Zucolotto, The use of dihexadecylphosphate in sensing and biosensing, *Sens. Actuators, B*, 2015, **220**, 805–813.

15 A. Domenech-Carbo, L. M. de Carvalho, M. Martini and G. Cebrian-Torrejon, Voltammetric/amperometric screening of compounds of pharmacological interest, *Rev. Anal. Chem.*, 2014, **33**, 173–199.

16 K. Kalcher, Chemically Modified Carbon Paste Electrodes in Voltammetric Analysis, *Electroanalysis*, 1990, **2**, 419–433.

17 G. Gasparotto, M. A. Cebim, M. S. Goes, S. A. M. Lima, M. R. Davolos, J. A. Varela, C. O. Paiva-Santos and M. A. Zaghete, Correlation between the spectroscopic and structural properties with the occupation of Eu^{3+} sites in powdered Eu^{3+}-doped $LiTaO_3$ prepared by the Pechini method, *J. Appl. Phys.*, 2009, **106**, 063509.

18 M. R. Ganjali, M. R. Moghaddam, M. Hosseini and P. Norouzi, A Nano-composite Carbon Paste Lanthanum(III) Sensor, *Int. J. Electrochem. Sci.*, 2011, **6**, 1981–1990.

19 C. P. Montgomery, B. S. Murray, E. J. New, R. Pal and D. Parker, Cell-Penetrating Metal Complex Optical Probes: Targeted and Responsive Systems Based on Lanthanide Luminescence, *Acc. Chem. Res.*, 2009, **42**, 925–937.

20 J. C. G. Bunzli, Lanthanide Luminescence for Biomedical Analyses and Imaging, *Chem. Rev.*, 2010, **110**, 2729–2755.

21 S. Comby and T. Gunnlaugsson, Luminescent Lanthanide-Functionalized Gold Nanoparticles: Exploiting the Interaction with Bovine Serum Albumin for Potential Sensing Applications, *ACS Nano*, 2011, **5**, 7184–7197.

22 M. I. J. Stich, M. Schaeferling and O. S. Wolfbeis, Multicolor Fluorescent and Permeation-Selective Microbeads Enable Simultaneous Sensing of pH, Oxygen, and Temperature, *Adv. Mater.*, 2009, **21**, 2216–2220.

23 C. L. Tan and Q. M. Wang, Reversible Terbium Luminescent Polyelectrolyte Hydrogels for Detection of H_2PO_4- and HSO_4- in Water, *Inorg. Chem.*, 2011, **50**, 2953–2956.

24 P. A. Raymundo-Pereira, M. F. S. Teixeira, O. Fatibello, E. R. Dockal, V. G. Bonifacio and L. H. M. Lino, Electrochemical sensor for ranitidine determination based on carbon paste electrode modified with oxovanadium(IV) salen complex, *Mater. Sci. Eng., C*, 2013, **33**, 4081–4085.

25 Q. L. Sheng, K. Luo, J. B. Zheng and H. F. Zhang, Enzymatically induced formation of neodymium hexacyanoferrate nanoparticles on the glucose oxidise/

chitosan modified glass carbon electrode for the detection of glucose, *Biosens. Bioelectron.*, 2008, **24**, 429–434.

26 Y. Li, Y. F. Gao, Y. Zhou, Y. C. Liu and J. R. Liu, Glucose oxidase-Tm_2O_3 nanoparticle-modified electrode for direct electrochemistry and glucose sensing, *J. Electroanal. Chem.*, 2010, **642**, 1–5.

27 Y. Y. Shao, J. Wang, H. Wu, J. Liu, I. A. Aksay and Y. H. Lin, Graphene Based Electrochemical Sensors and Biosensors: A Review, *Electroanalysis*, 2010, **22**, 1027–1036.

28 M. F. Bergamini, M. F. S. Teixeira, E. R. Dockal, N. Bocchi and E. T. G. Cavalheiro, Evaluation of different voltammetric techniques in the determination of amoxicillin using a carbon paste electrode modified with [*N*,*N*′-ethylenebis(salicylideneaminato)] oxovanadium(IV), *J. Electrochem. Soc.*, 2006, **153**, E94–E98.

29 M. F. S. Teixeira, L. H. Marcolino-Junior, O. Fatibello-Filho, E. R. Dockal and M. F. Bergamini, An electrochemical sensor for (L)-dopa based on oxovanadium-salen thin film electrode applied flow injection system, *Sens. Actuators, B*, 2007, **122**, 549–555.

30 S. Thirurnalairajan, K. Girija, V. Ganesh, D. Mangalaraj, C. Viswanathan and N. Ponpandian, Novel Synthesis of $LaFeO_3$ Nanostructure Dendrites: A Systematic Investigation of Growth Mechanism, Properties, and Biosensing for Highly Selective Determination of Neurotransmitter Compounds, *Cryst. Growth Des.*, 2013, **13**, 291–302.

31 L. S. de Oliveira, M. A. Balbino, M. M. T. de Menezes, E. R. Dockal and M. F. de Oliveira, Voltammetric analysis of cocaine using platinum and glassy carbon electrodes chemically modified with Uranyl Schiff base films, *Microchem. J.*, 2013, **110**, 374–378.

32 M. F. S. Teixeira, L. H. Marcolino-Junior, O. Fatibello, E. R. Dockal and E. T. G. Cavalheiro, Voltammetric determination of dipyrone using a *N*,*N*′-ethylenebis-(salicylideneaminato)oxovanadium(IV) modified carbon-paste electrode, *J. Braz. Chem. Soc.*, 2004, **15**, 803–808.

33 P. Norouzi, F. Dousty, M. R. Ganjali and P. Daneshgar, Dysprosium Nanowire Modified Carbon Paste Electrode for the Simultaneous Determination of Naproxen and Paracetamol: Application in Pharmaceutical Formulation and Biological Fluid, *Int. J. Electrochem. Sci.*, 2009, **4**, 1373–1386.

34 M. L. Rodríguez-Méndez, V. Parra, C. Apetrei, S. Villanueva, M. Gay, N. Prieto, J. Martinez and J. A. de Saja, Electronic tongue based on voltammetric electrodes modified with materials showing complementary electroactive properties. Applications, *Microchim. Acta*, 2008, **163**, 23–31.

35 *The Sol–Gel Handbook: Synthesis, Characterization, and Applications*, ed. David Levy and Marcos Zayat, Wiley, 2015.

36 A. Birkel, N. A. DeCINO, N. C. Jorge, K. A. Hazelton, B. C. Hong and R. Seshardi, Eu^{2+}-Doped M_2SiO_4 (M = Ca, Ba) phosphors prepared by a rapid microwave assisted sol-gel method: phase formation and optical properties, *Solid State Sci.*, 2013, **19**, 51–57.

37 B. Ritter, T. Krahl, K. Rurack and E. Kemnitz, Nanoscale CaF_2 doped with Eu^{3+} and Tb^{3+} through fluorolytic sol-gel synthesis, *J. Mater. Chem. C*, 2014, **2**, 8607–8613.

38 J. El Ghoul, K. Omri, S. A. Gomez-Lopera and L. El Mir, Sol-gel synthesis, structural and luminescence properties of MT-doped SiO_2/Zn_2SiO_4 nanocomposites, *Opt. Mater.*, 2014, **36**, 1034–1039.

39 T. Fukumoto, T. Yoshioka, H. Nagasawa, M. Kanezashi and T. Tsuru, Development and gas permeation properties of microporous amorphous TiO_2–ZrO_2–organic composite membranes using chelating ligands, *J. Membr. Sci.*, 2014, **461**, 96–105.

40 P. A. Raymundo-Pereira, M. F. S. Teixeira, F. R. Caetano, M. F. Bergamini and L. H. Marcolino, A Simple and Rapid Estimation of Totals Polyphenols Based On Carbon Paste Electrode Modified with Ruthenium Oxo-Complex, *Electroanalysis*, 2015, **27**, 2371–2376.

41 R. K. Sharma, S. Gulati, A. Pandey and A. Adholeya, Novel, efficient and recyclable silica based organic–inorganic hybrid Nickel catalyst for degradation of dye pollutants in a newly designed chemical reactor, *Appl. Catal., B*, 2012, **125**, 247–258.

42 X. Rios, P. Moriones, J. C. Echeverria, A. Luquin, M. Laguna and J. J. Garrido, Characterisation of hybrid xerogels synthesised in acid media using methyltriethoxysilane (MTEOS) and tetraethoxysilane (TEOS) as precursors, *Adsorption*, 2011, **17**, 583–593.

43 K. Q. Ding, W. Y. Cai and Q. F. Wang, Cyclic Voltammetric Investigation of Eu^{3+} on a MWCNTs/SDS-Modified Glassy Carbon (GC) Electrode, *Russ. J. Electrochem.*, 2010, **46**, 180–187.

44 S. Ferro and A. De Battisti, Electrochemistry of the aqueous europium(III)/europium(II) redox couple at conductive diamond electrodes, *J. Electroanal. Chem.*, 2002, **533**, 177–180.

45 C. S. Martin, T. R. L. Dadamos and M. F. S. Teixeira, Development of an electrochemical sensor for determination of dissolved oxygen by nickel-salen polymeric film modified electrode, *Sens. Actuators, B*, 2012, **175**, 111–117.

46 P. Bertoncello and P. Ugo, Preparation and voltammetric characterization of electrodes coated with Langmuir-Schaefer ultrathin films of Nafion (R), *J. Braz. Chem. Soc.*, 2003, **14**, 517–522.

47 P. R. de Oliveira, M. M. Oliveira, A. J. G. Zarbin, L. H. Marcolino and M. F. Bergamini, Flow injection amperometric determination of isoniazid using a screen-printed carbon electrode modified with silver hexacyanoferrates nanoparticles, *Sens. Actuators, B*, 2012, **171**, 795–802.

48 F. R. Caetano, A. Gevaerd, E. G. Castro, M. F. Bergamini, A. J. G. Zarbin and L. H. Marcolino, Electroanalytical application of a screen-printed electrode modified by dodecanethiol-stabilized platinum nanoparticles for dapsone determination, *Electrochim. Acta*, 2012, **66**, 265–270.

